Check for updates

ADVANCING EARTH AND SPACE SCIENCES

Earth and Space Science

RESEARCH LETTER
10.1029/2024EA004176

Observations of Sea-Swell Wave Reflection From a Steep, Nearshore Bar

Drude F. Christensen[1,2], Britt Raubenheimer[2], and Steve Elgar[2]

[1]Department of Geosciences and Natural Resource Management, University of Copenhagen, Copenhagen, Denmark,
[2]AOPE Department, Woods Hole Oceanographic Institution, Woods Hole, MA, USA

Key Points:
- Sea-swell wave reflection coefficients of ~0.8 are observed on the crest of a shallow surfzone sandbar
- Strong reflection results in standing wave relationships between pressure and velocity at sea-swell frequencies
- Observed reflection coefficient trends are consistent with theories for wave propagation over a vertical bathymetric step and a trough

Correspondence to:
D. F. Christensen,
dc@ign.ku.dk

Citation:
Christensen, D. F., Raubenheimer, B., & Elgar, S. (2025). Observations of sea-swell wave reflection from a steep, nearshore bar. *Earth and Space Science*, *12*, e2024EA004176. https://doi.org/10.1029/2024EA004176

Received 21 DEC 2024
Accepted 21 MAR 2025

Author Contributions:
Conceptualization: Britt Raubenheimer, Steve Elgar
Formal analysis: Drude F. Christensen
Funding acquisition: Drude F. Christensen, Britt Raubenheimer, Steve Elgar
Investigation: Britt Raubenheimer, Steve Elgar
Methodology: Britt Raubenheimer, Steve Elgar
Visualization: Drude F. Christensen
Writing – original draft: Drude F. Christensen
Writing – review & editing: Drude F. Christensen, Britt Raubenheimer, Steve Elgar

Abstract Wave reflection near the beach affects the energy reaching the shore, surfzone wave conditions, and sediment transport. Many prior studies have shown strong reflection of infragravity (0.01 < frequency < 0.05 Hz) wave energy from steep foreshore slopes. Here, swell-frequency bores were observed propagating offshore across a shallow sandbar crest at low tide. Reflection coefficients (ratio of outgoing to incoming energy) estimated from pressure and velocity observations were large (~0.8) at the frequency of the sea-swell peak (0.07 Hz), especially at low tide when the water depth on the bar crest relative to that in the trough is smallest. The high observed sea-swell reflection may have been at least partly owing to interactions of the incident waves with the surfzone bathymetry, which included a steep drop from the bar crest into a narrow bar-trough at the alongshore location where the offshore bore propagation was observed.

Plain Language Summary Sea and swell waves (periods of 5–20 s) were observed to reflect strongly from a nearshore sandbar and deep trough onshore of the bar crest on a sandy Atlantic Ocean beach. In contrast, 100 m north of the sandbar-trough system reflection of sea and swell was weak. The observations suggest wave reflection may depend on the sandbar configuration.

1. Introduction

The transformation of nearshore incident waves affects the forces on shorelines and coastal infrastructure, surfzone flows, and transport of sediments and pollutants. The amount of energy reaching the shore depends on the amount of wave dissipation across the surfzone and reflection at complex bathymetry such as sandbars and reef edges. Waves propagating toward shore can be reflected from natural or constructed structures depending on the topography, wave characteristics, and water depths (Collins et al., 2024; Elgar et al., 1994; Schoonees et al., 2022). Reflected waves modulate the observed (total) wave heights (Elgar et al., 1997) and can be an important part of the nearshore energy budget (Almar et al., 2019; Sheremet et al., 2002). Reflected waves also affect undertow velocities (Martins et al., 2017), nonlinear interactions and wave shapes (Voermans et al., 2020), suspended sediment concentration and the phasing with orbital velocities (Miles et al., 2001), and net sediment transport and beach morphology, including cusps and bar-trough systems (Almar et al., 2018; Wright, 1982). However, wave reflection at sea-swell frequencies ($0.05 < f < 0.50$ Hz) is not accounted for in wave-averaged models such as SWAN (Booij et al., 1999) and XBeach (Roelvink et al., 2009), which often are used in nearshore studies (Zhang et al., 2021).

High reflected wave energy is observed at low wave frequencies (infragravity waves) ($f < 0.05$ Hz) on natural sandy beaches (Bertin et al., 2020; Brodie et al., 2015; Fiedler et al., 2018; Guedes et al., 2013; Raubenheimer et al., 1995; Tatavarti et al., 1988; and many others). The offshore propagating long waves may be "leaky", ultimately radiating across ocean basins or may become trapped ("edge waves") owing to refraction over the sloping beach or along the crest of a sandbar (Bogiatzis et al., 2020; Bryan et al., 1998; Elgar et al., 1994; Herbers et al., 1995; Matsuba et al., 2024; Rijnsdorp et al., 2021). The combined incident and reflected waves result in standing wave patterns, with nodes and anti-nodes (Elgar & Guza, 1985b; Guza & Thornton, 1985; Raubenheimer & Guza, 1996; Suhayda, 1974) that may result in rhythmic variations in sediment transport and morphology (Almar et al., 2018; Wright, 1982).

Short waves (swell and sea) often are assumed to be dissipated in the surfzone by wave breaking. However, near artificial structures such as breakwaters, seawalls, and revetments high reflectivity has been observed for a broad range of wave frequencies (Miles et al., 1997; Suh et al., 2001). Sea-swell wave reflection also may be significant owing to abrupt underwater seafloor features offshore of the surfzone, such as borrow pits and canyons (Bender &

10.1029/2024EA004176

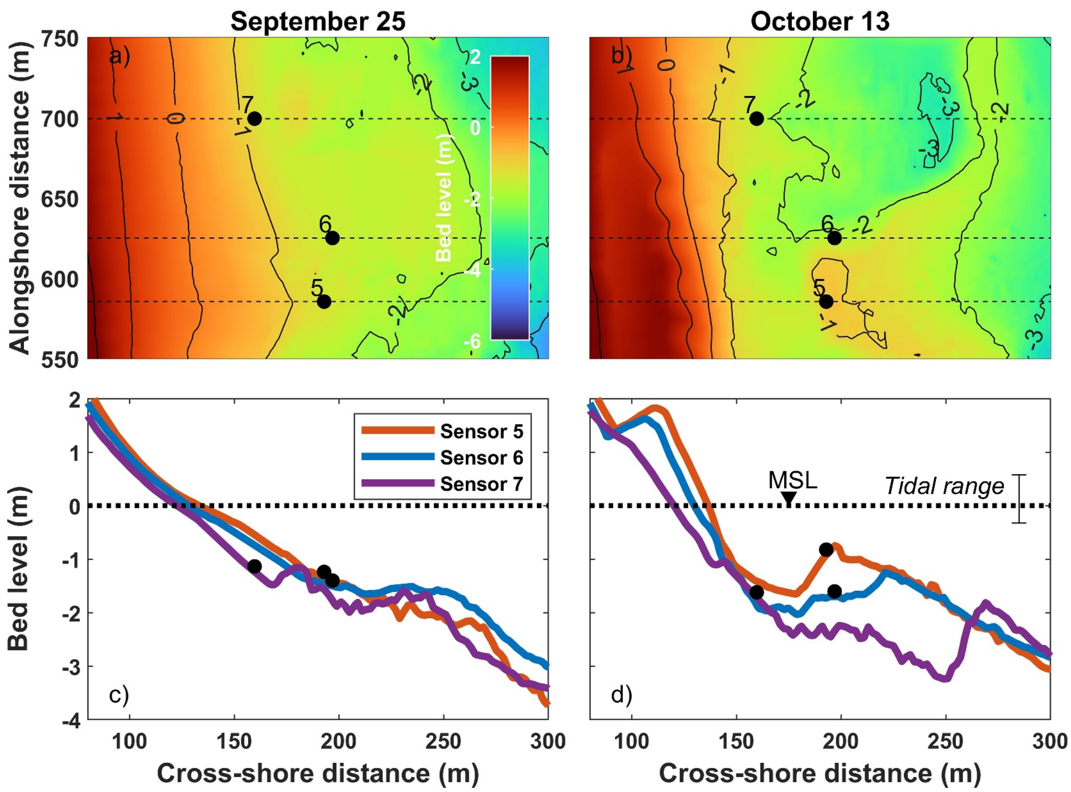

Figure 1. (a), (b) Bathymetry (color contours, scale on right) as a function of alongshore *y* and cross-shore *x* distance (north and offshore to the top and right, respectively) and (c), (d) bed levels (relative to NAVD88) along the horizontal dotted lines in (a) and (b) versus cross-shore distance (orange: $y = 585$ m, blue: $y = 625$ m, purple: $y = 700$ m) on (a), (c) September 25 and (b), (d) 13 October 2023. Black circles indicate horizontal positions (not the vertical elevations of the current meter sample volumes) of instruments labeled by the first number of the alongshore coordinate. The dashed, horizontal lines in (c) and (d) are mean sea level (MSL), with the vertical bar indicating the tidal range.

Dean, 2003, 2005; Magne et al., 2007; Michalsen et al., 2008). Although sea-swell reflection from coastal structures has gained attention due to the practical significance for ship navigation safety and structure destabilization through sediment scouring (Zanuttigh & Van Der Meer, 2007), there have been few studies of sea-swell reflection from natural sandy (relatively low-sloped) beaches (Martins et al., 2017).

Here, measurements of sea-surface elevation fluctuations and velocities obtained on a shallow sandbar are used to examine the relationship between sea-swell reflection and morphology of the bar-trough and sandy beach. Estimated surfzone reflection coefficients are compared with theories for wave reflection owing to abrupt changes in water depth.

2. Field Experiment

Pressure and velocity were measured at 2 Hz continuously between September 19 and 11 October 2023 at three sites within the surfzone (Figures 1a and 1b) on the sandy beach at the US Army Corps of Engineers Field Research Facility (FRF) on the Outer Banks, near Duck, NC, USA. Pressure gauges and Acoustic Doppler Velocimeters were installed on pipes jetted into the seabed with sample volumes initially about 0.6 m above the seafloor. A jet ski with a Global Positioning System and sonar (MacMahan, 2001; Moulton et al., 2014) was used for bathymetric surveys on September 25 and October 13. Diver-collected tape measurements of the sample volume height above sand were used with the surveys to estimate sensor elevation relative to NAVD88 and provided additional estimates of sand level changes. The elevation of sensor 5 was adjusted on Oct 10 at 11 a.m. resulting in a sample volume 0.25 m above the bed. Initially, the beach and nearshore bathymetry were almost alongshore uniform and gently sloping in the cross-shore (Figures 1a and 1c) with a foreshore slope (near the intersection of the bed level profile and mean sea level) of about 0.03. An emerging nearshore bar was observed

10.1029/2024EA004176

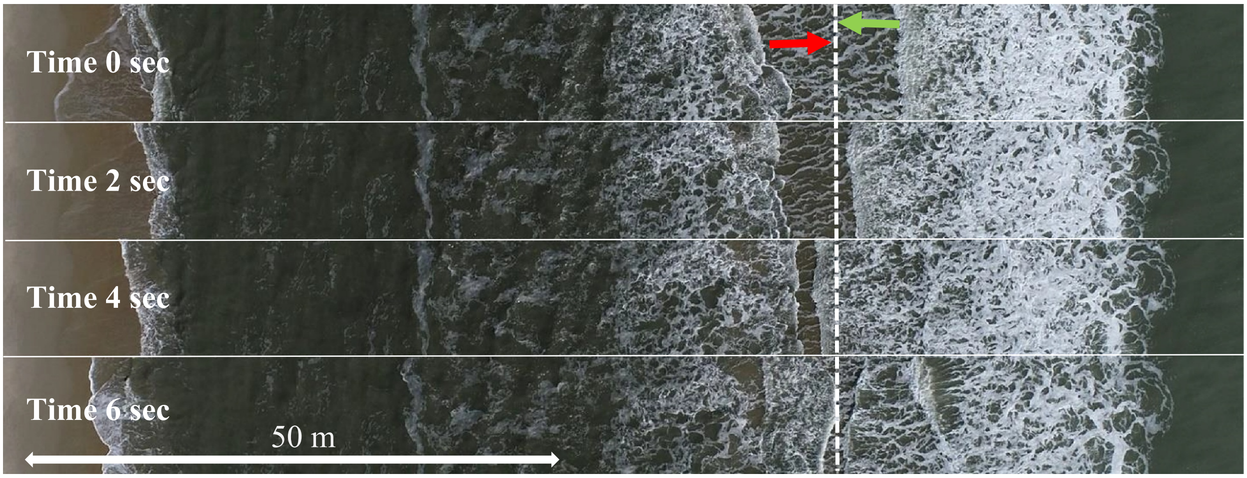

Figure 2. Four photographs each separated by 2 s showing onshore (green arrow) and offshore (red arrow) propagating bores crossing a shallow sandbar (highlighted by the white dashed line) near Duck, NC. The white arrow indicates the cross-shore scale.

visually starting on about October 7, and on October 13 a steep bar was surveyed in 0.75-m mean water depth at alongshore position (y) 550–625 m (Figures 1b and 1d). Simultaneously, the foreshore slope steepened to about 0.09 and surfers and swimmers experienced large offshore-directed bores crossing the shallow sandbar (Figure 2). Farther to the north ($y > 625$ m), the bar was in deeper water (1.8 m, Figures 1b and 1d) and was less pronounced.

Data are examined for two periods (September 21, 9 a.m. to September 22, 2 a.m. Local Time (LT), and October 10, 1 p.m. to October 11, 9 a.m. LT) as close in time as possible to the two different bathymetric surveys while ensuring similar wave conditions. Hourly time exposure images (Lippmann & Holman, 1990) suggest that wave breaking and morphology patterns did not change significantly between each survey and the corresponding analysis period. However, tape measurements showed the elevation of the bar crest changed up to 0.3 m between October 10 and 12. In addition, the sensors were observed to be on the bar crest on October 10–12, and just onshore of the crest on October 13 (Figure 1d). During the two periods, offshore (26-m water depth) wave conditions were nearly constant with significant wave height $H_s = 1$ m, peak period $T_p = 14$ s, and mean wave direction $MWD = 100°$N or about 17° south of normal incidence.

3. Theory

Assuming shore-normal linear long-waves, the wavefield is decomposed into incident and reflected waves using colocated pressure (p) and cross-shore velocity data (u). Incident ($\mathcal{F}_i$) and reflected ($\mathcal{F}_r$) energy fluxes are approximately (Sheremet et al., 2002):

$$\mathcal{F}_i = \frac{1}{4}C_g\left(Co_{pp}(f) + \frac{h}{g}Co_{uu}(f) + 2\sqrt{\frac{h}{g}}Co_{pu}(f)\right) \tag{1}$$

$$\mathcal{F}_r = \frac{1}{4}C_g\left(Co_{pp}(f) + \frac{h}{g}Co_{uu}(f) - 2\sqrt{\frac{h}{g}}Co_{pu}(f)\right) \tag{2}$$

where the group velocity $C_g = \sqrt{gh}$ with g being gravitational acceleration and h the total mean water depth (including setup). The terms Co_{pp} and Co_{uu} are p and u (positive is onshore) auto-spectra and Co_{pu} is the p-u cross-spectrum as a function of frequency f.

The pressure and velocity data were processed in 1800 s (30 min) segments and divided into 900 s sections with a 75% overlap. Each section was tapered with a Hanning window, demeaned, and quadratically detrended to reduce tidal leakage before auto- and cross-spectra were calculated. Five frequency bands were merged to achieve 20 degrees of freedom and a frequency resolution of 0.005 Hz. The wave reflection coefficient is calculated at the surfzone sensors as a function of frequency, $R^2(f)$, as (Brodie et al., 2015; Buckley et al., 2018; Elgar et al., 1997; Raubenheimer & Guza, 1996):

$$R^2(f) = \frac{\mathcal{F}_r}{\mathcal{F}_i} \tag{3}$$

and a bulk reflection coefficient integrated over sea-swell frequencies (0.05–0.20 Hz) as:

$$bulk\ R^2 = \frac{\int_{0.05Hz}^{0.2Hz} \mathcal{F}_r}{\int_{0.05Hz}^{0.2Hz} \mathcal{F}_i} \tag{4}$$

Noise in the pressure and velocity records may cause slight overestimation of reflection coefficients using this method (Tatavarti et al., 1988). However, bias is expected to be small for the data used here, which has coherence between incoming and reflected waves greater than 0.5 (Huntley et al., 1999).

Field-based estimates of the wave reflection coefficient, R^2, are compared with analytical estimates of R^2 from a vertical step down (from the crest of the sandbar into the trough) (Lamb, 1932; Lin & Liu, 2005):

$$R^2 = \left(\frac{1 - \sqrt{\frac{h_1}{h_2}}}{1 + \sqrt{\frac{h_1}{h_2}}} \right)^2 \tag{5}$$

where h_1 is the water depth at the top of the step (i.e., bar crest) and h_2 is the water depth at the bottom of the step (i.e., bar trough). Comparisons also are made with the analytical solution for R^2 owing to wave propagation over a trench or canyon (Kirby & Dalrymple, 1983; Thomson et al., 2005, 2007), which for normally incident waves is:

$$R^2 = \frac{\gamma}{1 + \gamma} \tag{6}$$

where

$$\gamma = \frac{(h_1 - h_2)^2}{4 h_1 h_2} sin^2 \left(\frac{2\pi}{T_p \sqrt{g h_2}} W \right) \tag{7}$$

Here h_1 is the water depth outside the trench or canyon (i.e., the bar crest) and h_2 is the water depth within the trench (i.e., bar trough), T_p is wave peak period ($T_p\sqrt{gh_2} = L$ is the shallow-water wavelength), and W is the width of the trench. For a fixed trough morphology and sea level (depths), the theory suggests reflection is maximum for $nL/4 = W$, where n is an odd number (i.e., when an odd multiple of the wavelength equals four times the trough width).

The bathymetric surveys occurred a few days after each of the two time periods for which hydrodynamic measurements are examined. Thus, the theoretical formulas are evaluated for the observed h_1 and $h_2 \pm 0.2$ m, where the range of bathymetric uncertainty is based on estimated survey errors of 0.05–0.10 m (due to bubbles and interpolation) in combination with hand measurements during inspections showing tidally modulated sand level accretion and erosion of up to 0.3 m. The width of the trough W (60 m) is estimated as the distance from the bar crest to the shoreline at mean sea level (i.e., W is independent of tidal variations, consistent with a vertical step down into the trough and a vertical foreshore slope). A constant peak wave period ($T_p = 14$ s) is used given the near constant conditions during the two observational periods (standard deviations of 1.0 and 0.7 s, respectively, excluding the last 3 hours of the first period). During September 21, 11 p.m. to September 22, 2 a.m. T_p decreased by about a factor 2 without an observed change in the estimated reflection coefficients.

4. Results

Despite the similar incident wave conditions during September 21–22 and October 10–11 (compare Figure 3a with Figure 3b), wave reflection coefficients differ considerably, especially at sea-swell frequencies (compare Figure 3c with Figure 3d). On September 21–22, similar to prior observations of wave reflection from beaches

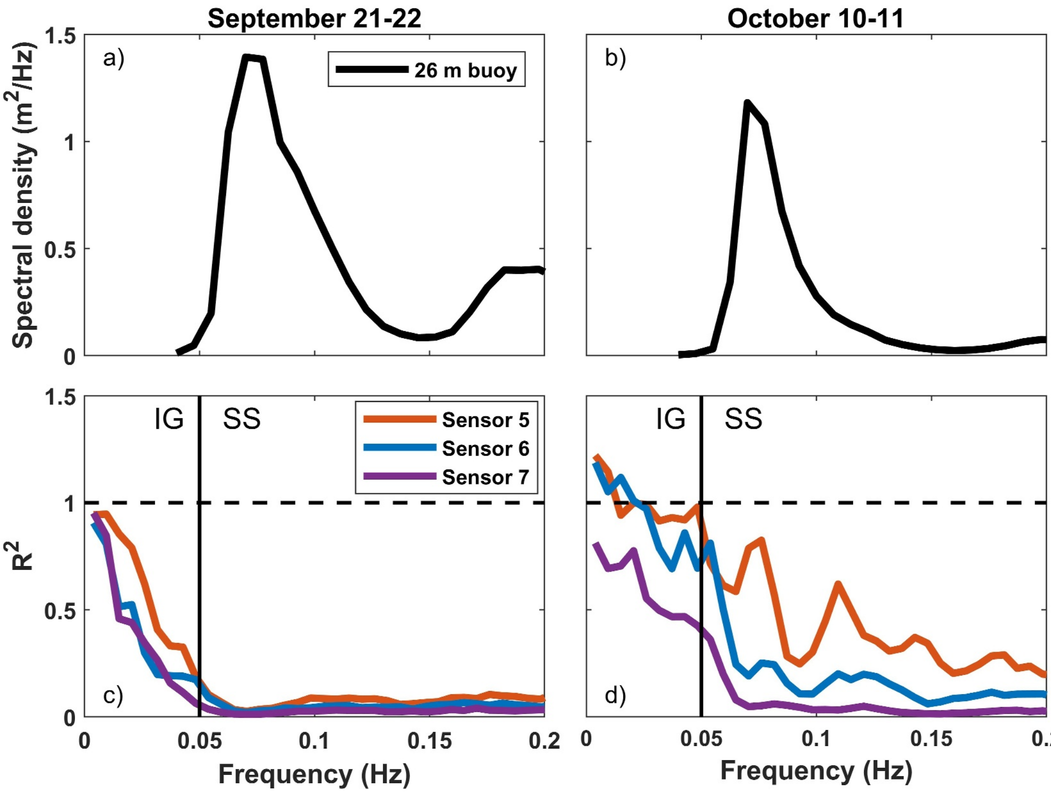

Figure 3. Average spectral density in 26-m water depth versus frequency on (a) September 21–22 and (b) October 10–11, and average wave reflection coefficient (R^2) versus frequency on (c) September 21–22 and (d) October 10–11 at sensor 5 (orange), 6 (blue), and 7 (purple). Vertical lines at $f = 0.05$ Hz separate infragravity (IG) and sea-swell (SS) wave frequencies. Dashed horizontal lines are R^2 equal one.

(Raubenheimer et al., 1995) $R^2 = 1$ for the lowest frequency infragravity waves and decreases with increasing frequency, with $R^2 < 0.2$ at sea-swell frequencies at all sensors (Figure 3c). The reflection coefficients are higher at all frequencies and all sensors on October 10–11 relative to those on September 21–22 (compare Figure 3d with Figure 3c). The IG reflection coefficients greater than 1 may result from nonlinear wave generation onshore of the measurement location (Bertin et al., 2020; Fiedler et al., 2018; Sheremet et al., 2002; Thomson et al., 2006). In addition, on October 10–11 at the incident peak period ($f = 0.07$ Hz) a local maximum exists with $R^2 \approx 0.8$ at sensor 5. Bispectral analysis (Elgar & Guza, 1985a) suggests that the motions at $f \sim 0.15$ Hz (and 0.22 Hz) are nonlinearly phase coupled harmonics (not shown) of motions at the spectral peak ($f = 0.07$ Hz). In contrast, sea-surface fluctuations at $f \sim 0.12$ Hz are not bound to motions at the peak frequency. The relatively high reflection coefficients at $f \sim 0.20$ Hz (compared with September 21–22 and with prior studies) could indicate a noise floor or accuracy level for the estimates (reflection coefficients are roughly constant for $0.20 < f < 1.00$ Hz, not shown).

The higher infragravity R^2 on October 10–11 is qualitatively consistent with the steeper foreshore beach slope (compare Figure 1d with Figure 1c) (Da Silva et al., 2019; Elgar et al., 1994; Raubenheimer & Guza, 1996). However, the reflection coefficient at the spectral peak (~0.07 Hz) is much higher than reported in prior studies. Moreover, on October 13 the foreshore beach slopes were similar at sensors 5 and 6 (Figure 1d), but R^2 at 0.07 Hz is significantly larger at sensor 5 ($R^2 = 0.8$, orange curve in Figure 3d), which was located on the steep sandbar (Figures 1b and 1d), than at sensor 6 ($R^2 = 0.25$, blue curve in Figure 3d), located north of the steep sandbar (Figures 1b and 1d). In addition, time series of incoming and reflected sea-swell ($0.05 < f < 0.20$ Hz) energy fluxes (Figure 4) show similar amounts of incoming wave energy at sensors 5 and 6, but larger reflected energy flux at sensor 5. Thus, it seems likely that the surfzone morphology is contributing to the high observed reflection over the bar.

The theories (Equations 5–7 applied to the October 10–11 bathymetry where a bar was present) suggest that reflection from a vertical step and from a trough increases with decreasing relative water level (i.e., as h_1/h_2

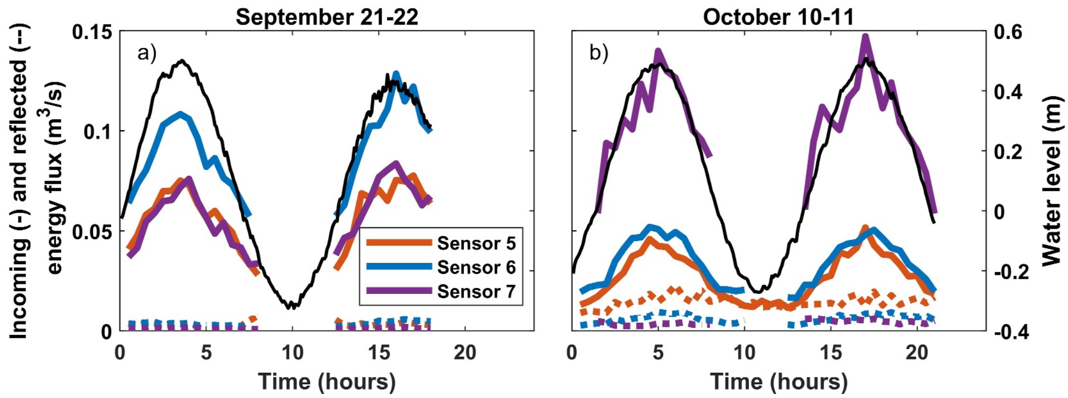

Figure 4. Water level (black, right y-axes) and sea-swell ($0.05 < f < 0.20$ Hz) incoming (solid curves) and reflected (dashed curves) energy fluxes (orange: sensor 5, blue: sensor 6, purple: sensor 7, left y-axes) versus time during (a) September 21–22 and (b) October 10–11.

approaches 0) (Figure 5c). Infragravity reflection is roughly constant with time during each period, and field-estimated IG reflection coefficients are uncorrelated with the theories (not shown). In contrast, the field-estimated sea-swell reflection coefficients R^2 at sensor 5 increase with decreasing tidal stage (Figure 5), qualitatively consistent with the theories. At sensors 6 and 7, theoretical R^2 values constantly were below 0.05 except for the trench solution for sensor 7. Due to the presence of a distinct bar offshore of sensor 7 (150 m from the shoreline) theoretical R^2 showed a peak of 0.09 (for observed bathymetry) at low tide (not shown). The trench theory (Equations 6 and 7) suggests reflection is maximum when $L = 4\ W/n$, where n is an odd number (sine-term in Equation 7 equals one). Thus, high reflection is expected for pairs of wavelengths with ratios of odd numbers

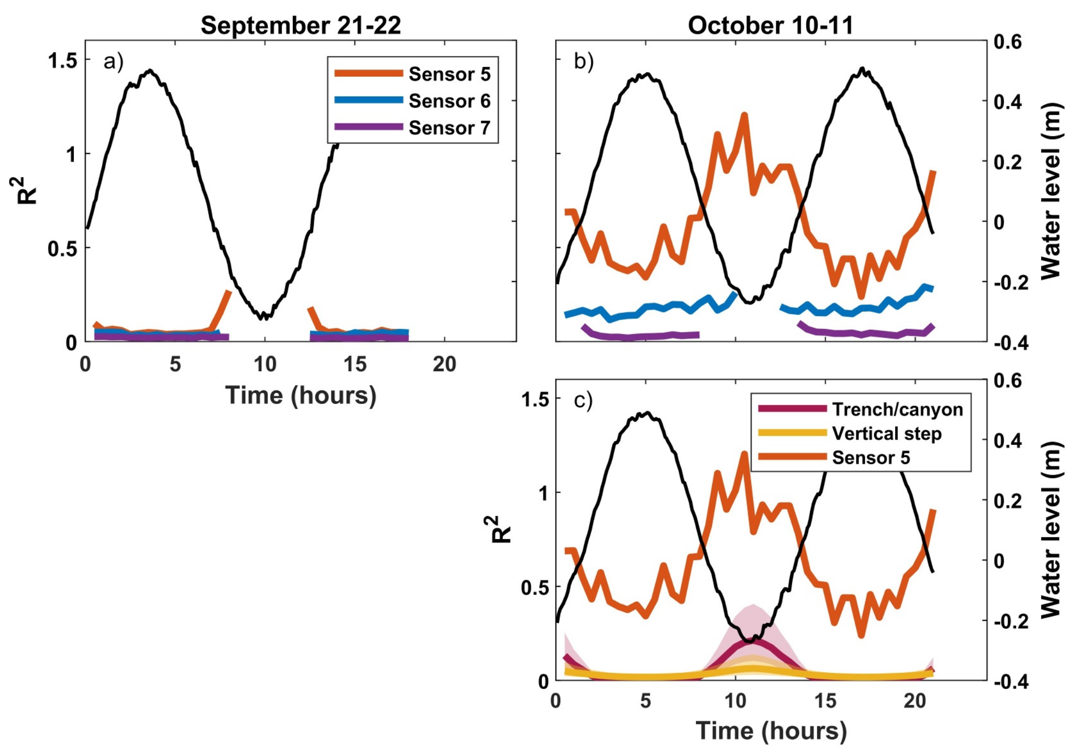

Figure 5. Water level (black, right y-axes) and sea-swell R^2 ($0.05 < f < 0.20$ Hz) (orange: sensor 5, blue: sensor 6, purple: sensor 7, left y-axes) versus time during (a) September 21–22 and (b), (c) October 10–11. Theoretical R^2 estimated using Equation 5 (dark red) and 4 (yellow) are included in (c). Shaded areas indicate the range of R^2 for the observed bathymetry ±0.2 m. Gaps in estimated R^2 occur when the sensors were not submerged during low tides. Sensor 5 was lowered 0.25 m prior to the October 10–11 time period.

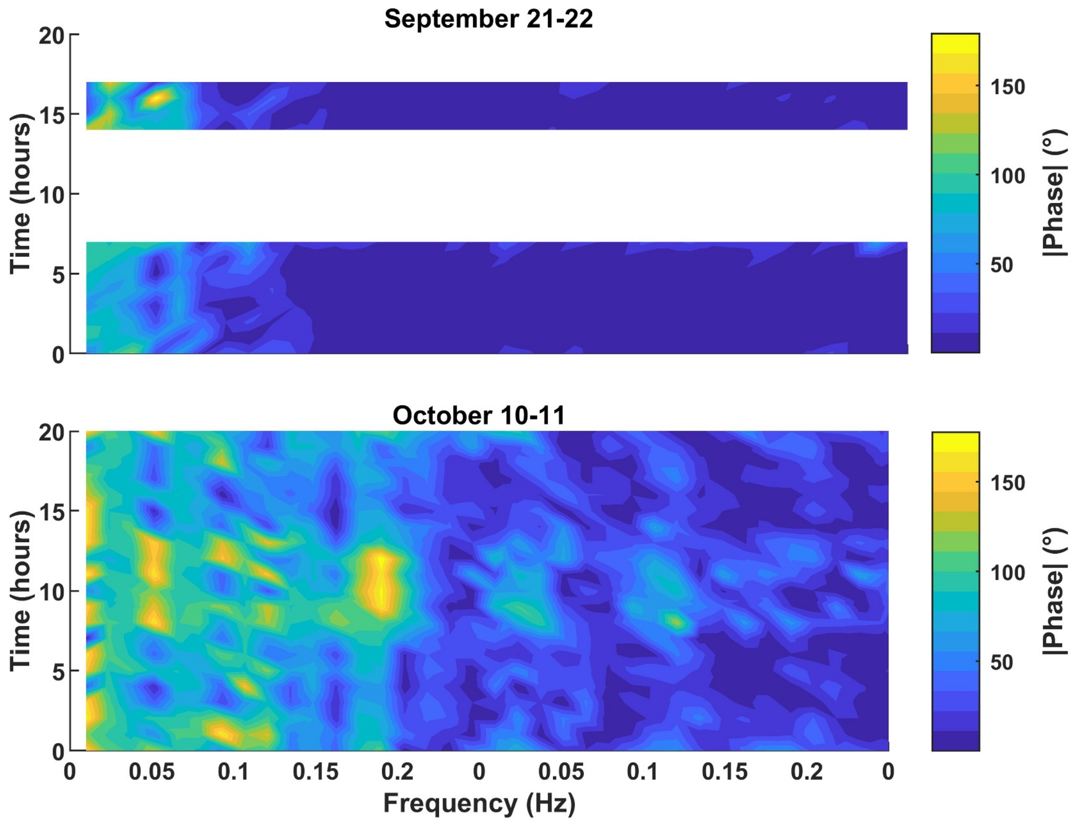

Figure 6. Color contours (scale on the right) of the phase between colocated pressure and cross-shore velocity measurements at sensor 5 as a function of time (y-axes) and frequency (x-axes) during (a) September 21–22 and (b) October 10–11. The gap (white region) in (a) occurs because sensor 5 was not submerged during low tide (the sensor was lowered prior to October 10).

(1/3, 3/5, and 5/7). The shallow-water wavelength ($L = T\sqrt{gh}$) of a 0.12 Hz wave (8.4 s period) is roughly 3/5 that of a 0.07 Hz wave (14 s period) for any constant water depth, and thus waves at both frequencies are expected to have strong reflection for similar bathymetric configurations, possibly explaining the small peak in reflection at ~0.12 Hz at sensor 5 (orange curve in Figure 3d). The field estimates are larger than the theoretical estimates, even accounting for potential inaccuracies in the bathymetry (shaded areas in Figure 5c). The relatively high field-based estimates could be owing to additional reflection from the foreshore slope, or to noisy estimates (possibly caused by flow nonlinearities). The sea-swell reflection coefficients estimated at high tide ($R^2 \sim 0.1$ to 0.4, Figures 5b and 5c hours 5 and 17) roughly are consistent with prior estimates on steep beaches (Anoop et al., 2014; Da Silva et al., 2019; Elgar et al., 1994; Martins et al., 2017; Miles & Russell, 2004; Raubenheimer & Guza, 1996). If these estimates represent the foreshore reflection or noise levels (i.e., minimum estimated R^2 owing to noisy velocities) and are removed from the field-based estimates, there would be better agreement between the observational estimates and theory. The overall theory-data agreement of the trends of R^2 with water level at sensor 5 suggests that the relative bar-trough water depth (Equation 5) or the interaction of the waves with the trough (Equation 6) could be important to sea-swell wave reflection.

A standing-wave structure in the phasing of colocated water surface (p) and cross-shore wave velocity ($\tilde{u}$) fluctuations (Elgar & Guza, 1985b; Guza & Thornton, 1985; Raubenheimer et al., 1995), with phases shifting between ±90° as a function of frequency, occurs at infragravity frequencies at both sensors 5 (Figure 6b) and 6 (not shown) on October 10–11, indicating strong reflection (near equal magnitudes of onshore and offshore propagating waves), possibly resulting from the steep shoreline (Figure 1d, orange and blue curves). The standing wave structure in the p-$\tilde{u}$ phases is observed to extend to sea-swell frequencies $f \geq 0.07$ Hz on October 10–11 only at sensor 5 (Figure 6b), consistent with a second source of reflection owing to the step from bar to trough. In contrast, during September 21–22, p-$\tilde{u}$ phases of approximately 90° are present only at low infragravity frequencies ($f < 0.03$ Hz, Figure 6a), above which the p-$\tilde{u}$ phase is near 0°, consistent with onshore propagating waves.

5. Discussion

Estimated reflection coefficients at the sea-swell peak were large (~0.8) at the position of a steep, nearshore bar (sensor 5). Prior studies have shown moderate sea-swell reflection due to steep foreshore slopes (Da Silva et al., 2019; Elgar et al., 1994). Here, foreshore slopes were similar at two positions in the surfzone (sensor 5 and 6) showing large and small reflection coefficients, respectively. Reflection coefficients in the surfzone also are affected by dissipation of incident wave energy offshore of the sensor location. As incident wave energy decreases (for sensors closer to the reflector), reflection coefficients increase. Incident wave energy was similar at sensors 5 and 6. The strong reflection coefficient estimated at the sea-swell peak on the crest of the shallow bar instead appears to be related to the steep onshore slope of the bar-crest and the relatively deep, narrow bar-trough. Although the values are lower, possibly owing to ratios of noisy estimates or some shoreline reflection, the qualitative agreement with theories for reflection from a vertical step and a trench or canyon thus suggests that surfzone bathymetry should be considered when evaluating wave reflection (Martins et al., 2017; Zhang et al., 2021). However, the effect of sandbars should be tested further in future studies because although the trends are similar, there are discrepancies between the theoretical and field estimated magnitudes of reflection coefficients.

The observed sea-swell reflection might be important to reducing the wave energy reaching the shore. Breaking wave dissipation typically dominates the attenuation of wave energy in the surfzone, including over a steep, shallow artificial bar (Li et al., 2023). However, the estimates here suggest optimal bar dimensions and position can result in significant wave reflection.

6. Conclusions

Strong reflection of waves in the sea-swell frequency band and the corresponding standing wave structures were observed at a natural sandy beach that included a shallow sandbar crest with a steep drop into a narrow trough between the bar and the shoreline. The high observed sea-swell reflection was at least partly owing to interactions of the incident waves with the surfzone bathymetry. Sea-swell reflection coefficients on the sandbar were maximum at low tide when the water depth on the bar crest relative to that in the trough was smallest and when the width of the bar-trough W was roughly equal to an odd multiple of quarter-wavelengths L of the incident waves ($L = 4W/n$, where n is an odd number), consistent with theories.

Data Availability Statement

The pressure, velocity, and bathymetry data used in this manuscript are available at https://doi.org/10.5281/zenodo.11179912 (Elgar & Raubenheimer, 2024). Offshore wave conditions were downloaded from the U.S. Army Corps of Engineers CHL Data Server (https://chlthredds.erdc.dren.mil/thredds/catalog/frf/catalog.html). Field data processing and figures were made in FORTRAN, IDL 9.0.0, and MATLAB R2023b.

Acknowledgments
We thank personnel at the U.S. Army Corps of Engineers Coastal Hydraulics Laboratory and members of the WHOI PVLAB Seth Ammons, Jinshi Chen, MP Delisle, Ciara Dooley, Austin Faddish, Levi Gorrell, Flo Grossman, Charles Murman, and Alexandra Muscalus for assistance collecting bathymetric surveys, and deploying, maintaining, and recovering the instruments despite being knocked over by reflected waves. Funding was provided by the Villum Foundation, the U.S. National Science Foundation, and the Office of Naval Research.

References

Almar, R., Blenkinsopp, C., Almeida, L. P., Catalán, P. A., Bergsma, E., Cienfuegos, R., & Viet, N. T. (2019). A new remote predictor of wave reflection based on runup asymmetry. *Estuarine, Coastal and Shelf Science*, *217*, 1–8. https://doi.org/10.1016/j.ecss.2018.10.018

Almar, R., Nicolae Lerma, A., Castelle, B., & Scott, T. (2018). On the influence of reflection over a rhythmic swash zone on surf zone dynamics. *Ocean Dynamics*, *68*(7), 899–909. https://doi.org/10.1007/s10236-018-1165-5

Anoop, T. R., Kumar, V. S., & Glejin, J. (2014). A study on reflection pattern of swells from the shoreline of peninsular India. *Natural Hazards*, *74*(3), 1863–1879. https://doi.org/10.1007/s11069-014-1282-5

Bender, C. J., & Dean, R. G. (2003). Wave transformation by two-dimensional bathymetric anomalies with sloped transitions. *Coastal Engineering*, *50*(1–2), 61–84. https://doi.org/10.1016/j.coastaleng.2003.08.002

Bender, C. J., & Dean, R. G. (2005). Wave transformation by axisymmetric three-dimensional bathymetric anomalies with gradual transitions in depth. *Coastal Engineering*, *52*(4), 331–351. https://doi.org/10.1016/j.coastaleng.2004.12.005

Bertin, X., Martins, K., De Bakker, A., Chataigner, T., Guérin, T., Coulombier, T., & De Viron, O. (2020). Energy transfers and reflection of infragravity waves at a dissipative beach under storm waves. *Journal of Geophysical Research: Oceans*, *125*(5), e2019JC015714. https://doi.org/10.1029/2019JC015714

Bogiatzis, P., Karamitrou, A., Ward Neale, J., Harmon, N., Rychert, C. A., & Srokosz, M. (2020). Source regions of infragravity waves recorded at the bottom of the equatorial Atlantic Ocean, using OBS of the PI-LAB experiment. *Journal of Geophysical Research: Oceans*, *125*(6), e2019JC015430. https://doi.org/10.1029/2019JC015430

Booij, N., Ris, R. C., & Holthuijsen, L. H. (1999). A third-generation wave model for coastal regions: 1. Model description and validation. *Journal of Geophysical Research*, *104*(C4), 7649–7666. https://doi.org/10.1029/98JC02622

Brodie, K. L., Raubenheimer, B., Elgar, S., Slocum, R. K., & McNinch, J. E. (2015). Lidar and pressure measurements of inner-surfzone waves and setup. *Journal of Atmospheric and Oceanic Technology*, *32*(10), 1945–1959. https://doi.org/10.1175/JTECH-D-14-00222.1

Bryan, K. R., Howd, P. A., & Bowen, A. J. (1998). Field observations of bar-trapped edge waves. *Journal of Geophysical Research*, *103*(C1), 1285–1305. https://doi.org/10.1029/97jc02938

Buckley, M. L., Lowe, R. J., Hansen, J. E., Van Dongeren, A. R., & Storlazzi, C. D. (2018). Mechanisms of wave-driven water level variability on reef-fringed coastlines. *Journal of Geophysical Research: Oceans*, *123*(5), 3811–3831. https://doi.org/10.1029/2018JC013933

Collins, P., MacMahan, J., Thornton, E., Benbow, C., & Jessen, P. (2024). Beach and Backward Bragg Sea-Swell wave reflection across rocky and sandy shores. *Journal of Geophysical Research: Oceans*, *129*(11), e2023JC020177. https://doi.org/10.1029/2023JC020177

Da Silva, P. G., Medina, R., González, M., & Garnier, R. (2019). Wave reflection and saturation on natural beaches: The role of the morphodynamic beach state in incident swash. *Coastal Engineering*, *153*, 103540. https://doi.org/10.1016/j.coastaleng.2019.103540

Elgar, S., & Guza, R. T. (1985a). Observations of bispectra of shoaling surface gravity waves. *Journal of Fluid Mechanics*, *161*(-1), 425–448. https://doi.org/10.1017/S0022112085003007

Elgar, S., & Guza, R. T. (1985b). Shoaling gravity waves: Comparisons between field observations, linear theory, and a nonlinear model. *Journal of Fluid Mechanics*, *158*, 47–70. https://doi.org/10.1017/s0022112085002543

Elgar, S., Guza, R. T., Raubenheimer, B., Herbers, T. H. C., & Gallagher, E. L. (1997). Spectral evolution of shoaling and breaking waves on a barred beach. *Journal of Geophysical Research*, *102*(C7), 15797–15805. https://doi.org/10.1029/97JC01010

Elgar, S., Herbers, T. H. C., & Guza, R. T. (1994). Reflection of ocean surface gravity waves from a natural beach. *Journal of Physical Oceanography*, *24*(7), 1503–1511. https://doi.org/10.1175/1520-0485(1994)024<1503:roosgw>2.0.co;2

Elgar, S., & Raubenheimer, B. (2024). SINKEX PUV and survey data (FRF 2023). *Zenodo*. https://doi.org/10.5281/zenodo.11179912

Fiedler, J. W., Smit, P. B., Brodie, K. L., McNinch, J., & Guza, R. T. (2018). Numerical modeling of wave runup on steep and mildly sloping natural beaches. *Coastal Engineering*, *131*, 106–113. https://doi.org/10.1016/j.coastaleng.2017.09.004

Guedes, R. M. C., Bryan, K. R., & Coco, G. (2013). Observations of wave energy fluxes and swash motions on a low-sloping, dissipative beach: Wave Energy Fluxes and Swash Motions. *Journal of Geophysical Research: Oceans*, *118*(7), 3651–3669. https://doi.org/10.1002/jgrc.20267

Guza, R. T., & Thornton, E. B. (1985). Observations of surf beat. *Journal of Geophysical Research*, *90*(C2), 3161–3172. https://doi.org/10.1029/JC090iC02p03161

Herbers, T. H. C., Elgar, S., Guza, R. T., & O'Reilly, W. C. (1995). Infragravity-frequency (0.005-0.05 Hz) motions on the Shelf. Part II: Free waves. *Journal of Physical Oceanography*, *25*(6), 1063–1079. https://doi.org/10.1175/1520-0485(1995)025<1063:ifhmot>2.0.co;2

Huntley, D. A., Simmonds, D., & Tatavarti, R. (1999). Use of collocated sensors to measure coastal wave reflection. *Journal of Waterway, Port, Coastal, and Ocean Engineering*, *125*(1), 46–52. https://doi.org/10.1061/(ASCE)0733-950X(1999)125:1(46)

Kirby, J. T., & Dalrymple, R. A. (1983). Propagation of obliquely incident water waves over a trench. *Journal of Fluid Mechanics*, *133*, 47–63. https://doi.org/10.1017/S0022112083001780

Lamb, H. (1932). *Hydrodynamics* (6th ed., p. 427). Cambridge University Press. 1879-1932.

Li, Y., Wang, P., Li, Q., Dai, W., Zhao, B., Chen, D., & Zhang, C. (2023). Roles of breaking and reflection in wave energy attenuation on the shoreface-nourished beach. *Physics of Fluids*, *35*(8), 087108. https://doi.org/10.1063/5.0156764

Lin, P., & Liu, H.-W. (2005). Analytical study of linear long-wave reflection by a two-dimensional obstacle of general trapezoidal shape. *Journal of Engineering Mechanics*, *131*(8), 822–830. https://doi.org/10.1061/(ASCE)0733-9399(2005)131:8(822)

Lippmann, T. C., & Holman, R. A. (1990). The spatial and temporal variability of sand bar morphology. *Journal of Geophysical Research*, *95*(C7), 11575–11590. https://doi.org/10.1029/JC095iC07p11575

MacMahan, J. (2001). Hydrographic surveying from personal watercraft. *Journal of Surveying Engineering*, *127*(1), 12–24. https://doi.org/10.1061/(ASCE)0733-9453(2001)127:1(12)

Magne, R., Belibassakis, K. A., Herbers, T. H. C., Ardhuin, F., O'Reilly, W. C., & Rey, V. (2007). Evolution of surface gravity waves over a submarine canyon. *Journal of Geophysical Research*, *112*(C1), 2005JC003035. https://doi.org/10.1029/2005JC003035

Martins, K., Blenkinsopp, C. E., Almar, R., & Zang, J. (2017). The influence of swash-based reflection on surf zone hydrodynamics: A wave-by-wave approach. *Coastal Engineering*, *122*, 27–43. https://doi.org/10.1016/j.coastaleng.2017.01.006

Matsuba, Y., Roelvink, D., & Van Dongeren, A. (2024). Propagation of free infragravity waves generated at distant beaches. *Journal of Geophysical Research: Oceans*, *129*(10), e2023JC020580. https://doi.org/10.1029/2023JC020580

Michalsen, D. R., Haller, M. C., & Suh, K. D. (2008). Wave reflection from nearshore depressions. *Journal of Waterway, Port, Coastal, and Ocean Engineering*, *134*(1), 1–11. https://doi.org/10.1061/(ASCE)0733-950X(2008)134:1(1)

Miles, J. R., & Russell, P. E. (2004). Dynamics of a reflective beach with a low tide terrace. *Continental Shelf Research*, *24*(11), 1219–1247. https://doi.org/10.1016/j.csr.2004.03.004

Miles, J. R., Russell, P. E., & Huntley, D. A. (1997). Sediment transport and wave reflection near a seawall. *Coastal Engineering*, *1996*, 2612–2624. https://doi.org/10.1061/9780784402429.202

Miles, J. R., Russell, P. E., & Huntley, D. A. (2001). Field measurements of sediment dynamics in front of a seawall. *Journal of Coastal Research*, *17*.

Moulton, M., Elgar, S., & Raubenheimer, B. (2014). Improving the time resolution of surfzone bathymetry using in situ altimeters. *Ocean Dynamics*, *64*(5), 755–770. https://doi.org/10.1007/s10236-014-0715-8

Raubenheimer, B., & Guza, R. T. (1996). Observations and predictions of run-up. *Journal of Geophysical Research*, *101*(C11), 25575–25587. https://doi.org/10.1029/96JC02432

Raubenheimer, B., Guza, R. T., Elgar, S., & Kobayashi, N. (1995). Swash on a gently sloping beach. *Journal of Geophysical Research*, *100*(C5), 8751–8760. https://doi.org/10.1029/95JC00232

Rijnsdorp, D. P., Reniers, A. J. H. M., & Zijlema, M. (2021). Free infragravity waves in the north sea. *Journal of Geophysical Research: Oceans*, *126*(8), e2021JC017368. https://doi.org/10.1029/2021JC017368

Roelvink, D., Reniers, A., Van Dongeren, A., Van Thiel de Vries, J., McCall, R., & Lescinski, J. (2009). Modelling storm impacts on beaches, dunes and barrier islands. *Coastal Engineering*, *56*(11–12), 1133–1152. https://doi.org/10.1016/j.coastaleng.2009.08.006

Schoonees, T., Kerpen, N. B., & Schlurmann, T. (2022). Full-scale experimental study on wave reflection and run-up at stepped revetments. *Coastal Engineering*, *172*, 104045. https://doi.org/10.1016/j.coastaleng.2021.104045

Sheremet, A., Guza, R. T., Elgar, S., & Herbers, T. H. C. (2002). Observations of nearshore infragravity waves: Seaward and shoreward propagating components. *Journal of Geophysical Research*, *107*(C8). https://doi.org/10.1029/2001JC000970

Suh, K. D., Choi, J. C., Kim, B. H., Park, W. S., & Lee, K. S. (2001). Reflection of irregular waves from perforated-wall caisson breakwaters. *Coastal Engineering*, *44*(2), 141–151. https://doi.org/10.1016/S0378-3839(01)00028-X

10.1029/2024EA004176

Suhayda, J. N. (1974). Standing waves on beaches. *Journal of Geophysical Research*, *79*(21), 3065–3071. https://doi.org/10.1029/JC079i021p03065

Tatavarti, R. V. S. N., Huntley, D. A., & Bowen, A. J. (1988). Incoming and outgoing wave interactions on beaches. *Coastal Engineering*, 136–150. https://doi.org/10.1061/9780872626874.010

Thomson, J., Elgar, S., & Herbers, T. H. C. (2005). Reflection and tunneling of ocean waves observed at a submarine canyon. *Geophysical Research Letters*, *32*(10), 2005GL022834. https://doi.org/10.1029/2005GL022834

Thomson, J., Elgar, S., Herbers, T. H. C., Raubenheimer, B., & Guza, R. T. (2007). Refraction and reflection of infragravity waves near submarine canyons. *Journal of Geophysical Research*, *112*(C10), 2007JC004227. https://doi.org/10.1029/2007JC004227

Thomson, J., Elgar, S., Raubenheimer, B., Herbers, T. H. C., & Guza, R. T. (2006). Tidal modulation of infragravity waves via nonlinear energy losses in the surfzone. *Geophysical Research Letters*, *33*(5), 2005GL025514. https://doi.org/10.1029/2005GL025514

Voermans, J. J., Laface, V., Babanin, A. V., Romolo, A., & Arena, F. (2020). Standing wave field observations at a vertical wall. *Coastal Engineering*, *160*, 103749. https://doi.org/10.1016/j.coastaleng.2020.103749

Wright, L. (1982). Field observations of long-period, surf-zone standing waves in relation to contrasting beach morphologies. *Marine and Freshwater Research*, *33*(2), 181. https://doi.org/10.1071/MF9820181

Zanuttigh, B., & Van Der Meer, J. W. (2007). Wave reflection from coastal structures. *Coastal Engineering*, *2006*, 4337–4349. https://doi.org/10.1142/9789812709554_0364

Zhang, C., Li, Y., Zheng, J., Xie, M., Shi, J., & Wang, G. (2021). Parametric modelling of nearshore wave reflection. *Coastal Engineering*, *169*, 103978. https://doi.org/10.1016/j.coastaleng.2021.103978